

EFFECT OF DESIGN PARAMETERS ON THE ULTIMATE STRENGTH AND COLLAPSE BEHAVIOUR OF STIFFENED PANELS

Muhammad Imaduddin Hanif¹, Ristiyanto Adiputra^{2*}, Aditya Rio Prabowo^{1*}, Nurul Muhaya¹, Adnan Sandy Dwi Marta², Nurul Huda³, Hermes Carvalho⁴

¹ Department of Mechanical Engineering, Universitas Sebelas Maret, Surakarta 57126, Indonesia

² Research Center for Hydrodynamics Technology, National Research and Innovation Agency (BRIN), Surabaya 60112, Indonesia

³ National Institute for Aquatic Resources, Technical University of Denmark, Lyngby 2800, Denmark

⁴ Department of Structural Engineering, Federal University of Minas Gerais, Belo Horizonte, 31270-901, Brazil

* ristiyanto.adiputra@brin.go.id; aditya@ft.uns.ac.id

Research about stiffened panel applications in ships has massively progressed with the amount of several methods to analyze it. Various studies had been conducted on stiffened panels using Finite Element Method (FEM). However, none have thoroughly explored the most optimal and efficient analysis methods and settings. Given the growing importance of FEM in reliability analysis for ship structures, particularly stiffened panels, a comprehensive study comparing different approaches is of paramount significance. Such research would not only streamline time-consuming procedures but also offer invaluable recommendations to advance the field's understanding and practical applications. In this paper, a finite element analysis study was done to analyze the influence of several parameter modeling of stiffened panels not only to achieve the models' ultimate strength value and collapse behavior but also to offer practical recommendations on the most optimal and efficient methods for analyzing stiffened panels through FEM. Conducting modification of three variations of the model configuration, four variations of boundary condition, and four variations of transverse stiffener modeling to compare each other. Running time consumed when simulations are calculated in ANSYS APDL was also being considered. The results showed a significant difference in modifying the model configuration's case, while in contrast, the modification of boundary conditions and transverse stiffener modeling only showed a slight difference in ultimate strength value. In addition, modification of transverse stiffener geometry only gave the difference by around 0.5 MPa. The model configuration case (A1 v A2) showed the most remarkable running time difference, which reached six times difference.

Keywords: stiffened panel, model configuration, boundary condition, transverse stiffener modelling, finite element method

NOMENCLATURES

Symbols/Name	Units	Description
a	mm	Span length
B_0	m	Amplitude for column and torsional imperfection mode
b	mm	Bay length
C_0	mm	Amplitude for local imperfection mode
E	N/mm ²	Young's Modulus
hs		Highest z coordinate of stiffened panel
m		Critical half-wave number at span
t_p	mm	Plate thickness
U	mm	Displacement
x, y, z		Element coordinate
W_l	mm	Maximum value of the local imperfection mode
W_t	mm	Maximum value of the torsional imperfection mode
W_c	mm	Maximum value of the column imperfection mode
β_p		Plate slenderness
ε		Strain
ε_y		Yield strain
σ	MPa	Strength
σ_{yield}, σ_y	MPa	Yield strength

1 INTRODUCTION

The stiffened panel is one part of a bulk carrier ship that plays an essential role in supporting the strength of the structure. The structure can increase strength by using stiffened panels without significantly increasing weight [1]. Structural reinforcement was carried out due to several accidents caused by structural failure to impinge on bulk carriers [2-3]. In Wei's research [2], for bulk carriers, there have been several major accidents occur on bulk carrier recorded during the 1970s to 1990. About a decade ago, from 2011 to 2020, a study by Nwigwe [3] noted that there was a total of 34 accidents that happened to bulk carriers and one of which was caused by structural failure. Roberts [4] noted that in 2001, a bulk carrier experienced structural failure causing death in 10 lives. Prior to a previous one, data from Kaddour [5] mentioned that in the six-year period between 1991 and 1996, there were a total of about 490 lives lost due to bulk carrier structural failures. Knowing the huge potential impact, therefore, strengthening the ship's structure through stiffened panels is necessary to be carried out so that loss of lives due to structural failure accidents can be prevented. Currently, in addition to analysis with experimental methods [6], approaches with Finite Element (FE) analysis are also carried out [6-7] and empirical calculation [8-13] in evaluating the strength of stiffened panels. IACS issued a rule that adopts the Ultimate Limit State (ULS) method in determining the safety of bulk carriers [14].

Finite Element Method (FEM) can be done without having to do complicated manufacturing and preparation, as is done with experimental methods. However, some variations in modeling aspects in FEM, such as determining the type of material, model material, meshing size, and setting boundary conditions, need to be considered because they can provide differences in one method with another. Various approaches are carried out, one of which is the model's configuration. Figure 1(a) shows simple modeling of stiffened panels with $1/2 + 1/2$ bay – $1/2 + 1/2$ span model configuration [8]. More extensive modeling was carried out by [15] with one and two-half model configurations on bay and span in comparing experimental and FE analysis methods, as seen in Figure 1(b). In 2018 with symmetric boundary conditions, [16] found a difference in normalized strength values of 0.15 compared to the two models where the most extensive configuration has the most significant value. However, in his research, the validity of the data could not be ascertained because the number of models compared was only two.

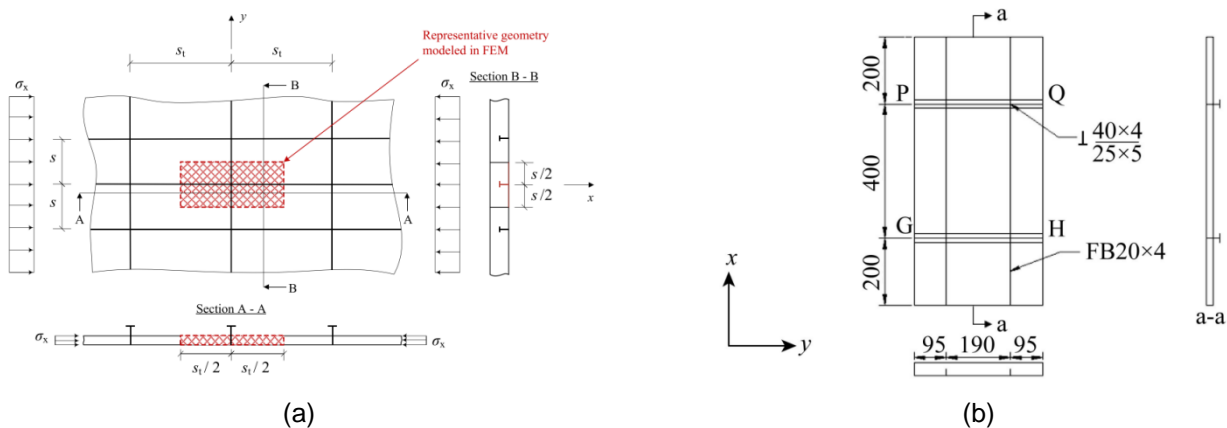


Figure 1: Previous model configuration, (a) $1/2 + 1/2$ bay – $1/2 + 1/2$ span [8], (b) $1/2 + 1 + 1/2$ bay – $1/2 + 1 + 1/2$ span [15].

Boundary conditions are the next aspect to be studied, such as in research conducted between [8] and [17] with significant differences in imposed location. Successively, the provision of forced displacement in the first case is carried out only at one end of the transverse edge. In contrast, in the second case, it is applied to one node at each end of the transverse edge with uniform conditions given coupling on the edge. In 2023, Adiputra et al. [18] provided the same imposed displacement as Anyfantis [8]. However, there are differences, where the transverse frame modeling, he does is only represented by fixing constraints on displacement on the z-axis.

Research on the comparison of periodic boundary conditions with symmetric boundary conditions was conducted by [19] on various loading conditions and their effects on the value of ultimate strength and collapse behavior. Furthermore, the periodic boundary condition was found to be the most suitable method because it was able to obtain appropriate results both in conditions with odd and even critical half-wave numbers. At the same time, symmetric only achieved the appropriate result if the value was equal to three. Meanwhile, in many of the stiffened panel studies mentioned earlier, the modeling of transverse stiffeners is often only represented in the form of constraints. Most are translated only by giving fixed conditions to displacement in the vertical direction. Based on those cases, the transverse stiffener did not experience column or local buckling when loaded. The provision of variations of the transverse stiffener model carried out by Platypodis and Anyfantis [6] is only limited to analyzing the maximum standard stress value, not to conducting parametric studies on the effect of the ultimate strength value. According to the above-mentioned explanations, it can be seen that various studies on stiffened panels have been carried out. However, none have studied the most optimal and efficient methods and settings for analyzing stiffened panels using FEM. This matter is crucial considering the current development of FEM to assist in conducting reliability analysis on ship structures, one of which is stiffened panels. Therefore, it is important to conduct a study that is able to provide a comparison of the various setting and methods offered so that it can provide recommendations regarding the one that represents the most optimal and efficient results so as to reduce the time consumption used.

In brief, the stiffened panel constructing the ship's hull girder has been widely studied. To investigate the effect of modeling uncertainties and to be able to provide recommendations on the most optimal and efficient method in the analysis of stiffened panels through FEM, in this research, modifications were made to Finite Element (FE) modeling by varying the provision of boundary conditions, the configuration of the model used, and the way of defining the transverse frame under the provision of uniform thrust. Four variations of boundary conditions, three variations of the model configuration, and four variations on how transverse frames are defined. The limitations in comparing boundary conditions and model configurations are imposed by assuming the application of fixed constraint conditions without modeling the transverse stiffener in 3D. The provision of initial geometric imperfection is carried out with three types of imperfection modes. Parametric studies were conducted to determine the effect on the value of ultimate strength and collapse behavior on stiffened panels, especially in parts affected by transverse frames, and determine the configuration and modeling suitable for analyzing stiffened panels numerically. In addition, parametric studies will consider the efficiency of the time required, given the importance of applying FE analysis to analyze many models.

2 METHODOLOGY

2.1 Research flowchart

The variation of various parameters was conducted based on references from several previous studies, enabling a comprehensive analysis. Figure 2 shows the flow of analysis in obtaining suitable analysis settings. Variance is done by varying the model configuration, boundary conditions, and transverse stiffener modeling. In the model configuration, several variations are used based on previous studies [8, 15, and 20]. The same thing was done in modifying boundary conditions by adopting previous studies [8, 17, 18, and 19]. Meanwhile, in the last variation in transverse stiffener modeling, the model without modeling the transverse stiffener was adopted from a study conducted by [18] and compared with a model by modeling a stiffener with a variation value based on a study conducted by [6]. The last step compared the value of ultimate strength, collapse behavior, and time efficiency when conducting FE analysis. In addition, all analyses were performed with ANSYS Parametric Design Language (APDL).

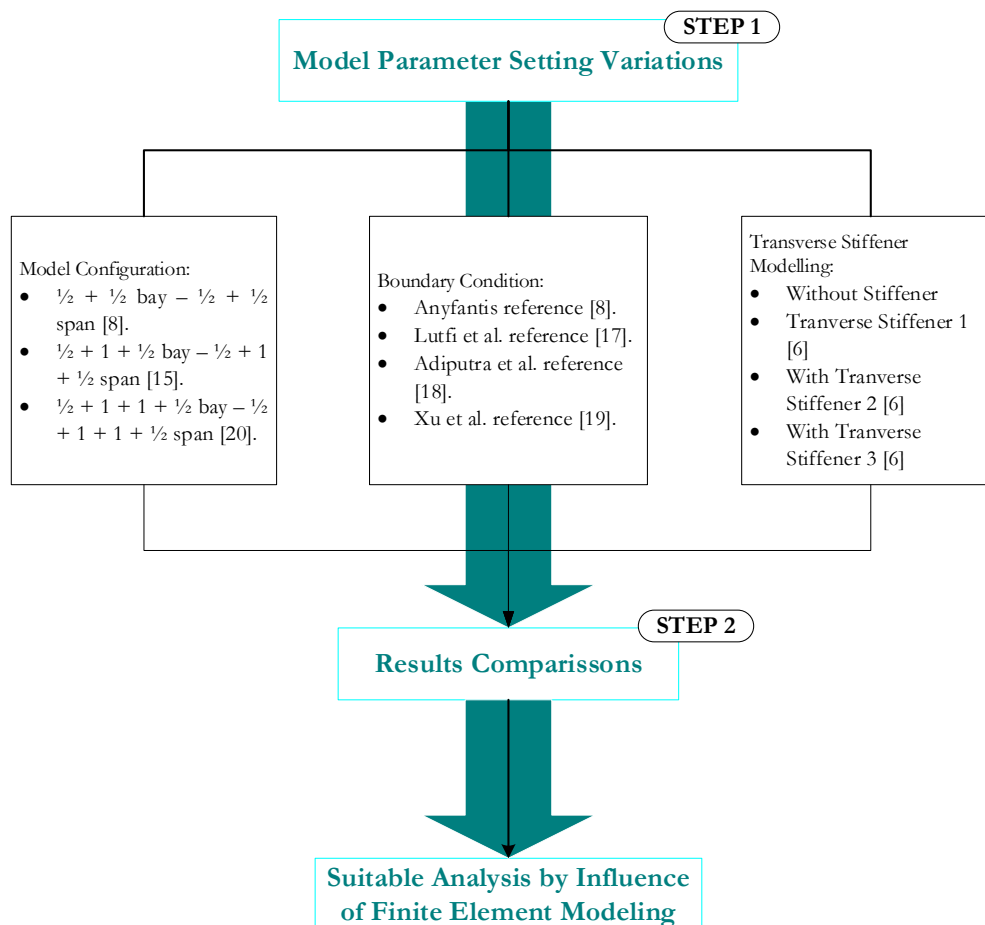


Figure 2: Research flowchart

2.2 Stiffened panel model size and properties

The ISSC (International Ship and Offshore Structures Congress) constitutes a globally recognized certification and pertinent report issued by the International Maritime Organization (IMO), encompassing 175 member countries and 3 associate members. As an active participant in maritime affairs, the ISSC strives to enhance safety in shipping

activities. The ISSC-2000 certification and report play a vital role in regulating safety and evaluating the structural integrity of vessels. Given the prevailing conditions, numerous cargo vessels, including Very Large Crude Carriers (VLCCs), oil tankers, and bulk carriers, face vulnerability to accidents, primarily attributed to structural failures. This research focused specifically on bulk carriers, seeking to investigate and address the findings and investigations mentioned earlier. Figure 3 shows the cross-sectional intersection of the hull bulk carrier taken from ISSC-2000 [21]. One of the studies analyzed by [22] showed a significant effect of double bottom bending strength of bulk carrier on the ultimate strength value, which had a correlation with the bottom plate. Because of its vital role, in this study, the analysis used the bottom plate, as shown by the red arrow.

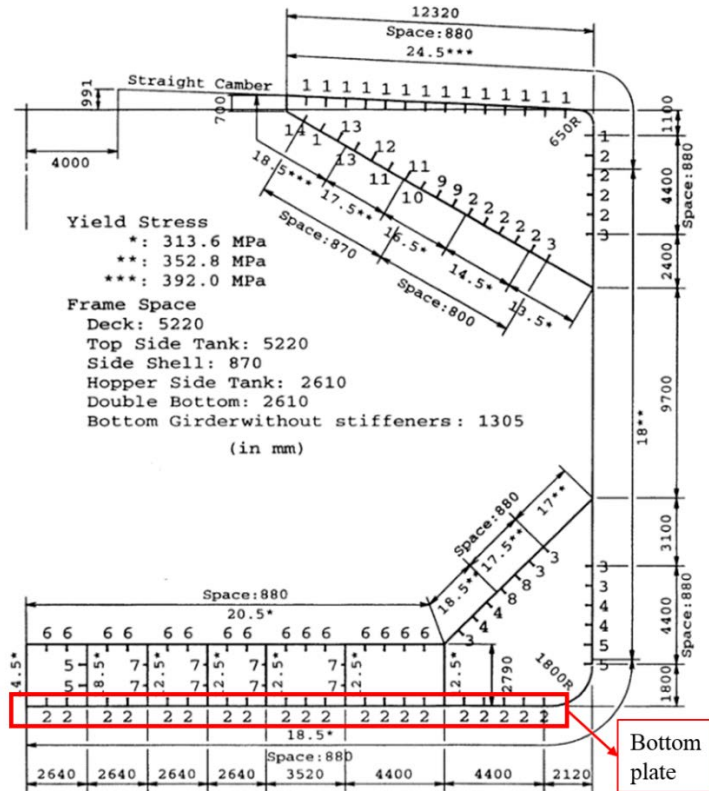


Figure 3: Hull girder cross-section and stiffened panel size of the ISSC-2000 bulk carrier

In this research, limitations were imposed on the type of stiffened panel model to be used, focusing on the tee-bar stiffened panel, as it constitutes a predominant structural element in the hull girder of bulk carriers. This selection allowed for a more representative analysis, considering that tee bars were extensively employed in the construction of bulk carrier hull structures. Details of the geometric of "Tee-bar" type stiffened panel in the double bottom are shown in Figure 4. The material properties used in modeling were high-strength steel with characteristics written in Table 1, which refers to [21].

Table 1. Material Properties of stiffened panel model

Properties	Value
Yield Strength [MPa]	352.8
Young's Modulus [MPa]	206,000
Poisson's Ratio	0.3
Plastic Tangent Modulus	0

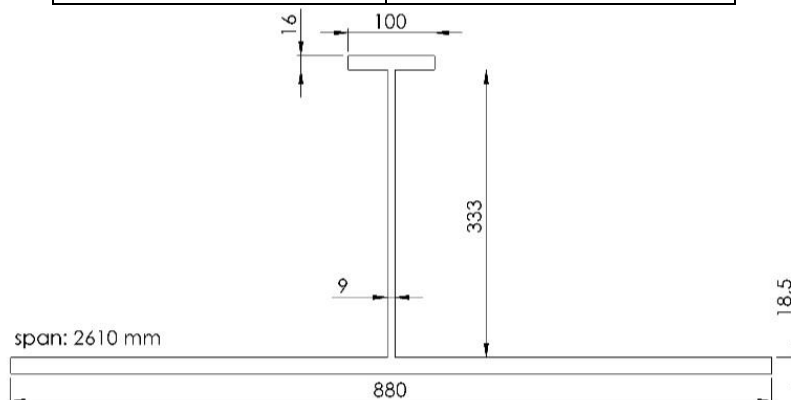


Figure 4: Stiffened panel dimensions (all units in mm)

2.3 Model configuration

The first variation will be done by modifying the range configuration model, as seen in Figure 5. Model modifications were made based on studies conducted by several previous researchers as described before using models 1/2 + 1/2 bay – 1/2 + 1/2 span, 1/2 + 1 + 1/2 bay – 1/2 + 1 + 1/2 span, and 1/2 + 1 + 1 + 1/2 bay – 1/2 + 1 + 1 + 1/2 span. The 1/2 + 1/2 bay - 1/2 + 1/2 span model was used in the Anyfantis study [8] because it was able to present the initial imperfection geometrics in the form of buckling modes under simply supported conditions. This was also performed in this paper by providing three imperfection modes in the form of column, torsional, and local imperfection modes. Yu, in other cases, used a model with 1/2 + 1 + 1/2 bay - 1/2 + 1 + 1/2 span because it has been widely used in determining the ultimate strength value influenced by plate and column slenderness. Meanwhile, the triple bay-triple span with 1/2 + 1 + 1 + 1/2 bay - 1/2 + 1 + 1 + 1/2 span configuration was modelled by Yao [20] because it yielded more rational deflection mode results. In addition, stiffened tee-bar panels with the mentioned configuration are applicable for buckling and plastic collapse behavior. Bay is the distance between two longitudinal bulkheads, while span is the distance between two bulkheads in the transverse direction. Longitudinal and transverse stiffeners are structural arrangements used as reinforcements in the hull of a ship, particularly in bulk carriers. The key distinction lies in the orientation, where longitudinal stiffeners run parallel to the keel of the ship, while transverse stiffeners are perpendicular to the keel. A more detailed depiction of the model range configuration for each model is presented in a 3D model view, as illustrated in Figure 6.

Table 2: Model range configuration's modification

Model	Model Range Configuration
A1	1/2 + 1/2 bay – 1/2 + 1/2 span
A2	1/2 + 1 + 1/2 bay – 1/2 + 1 + 1/2 span
A3	1/2 + 1 + 1 + 1/2 bay – 1/2 + 1 + 1 + 1/2 span

All models with half-half types along longitudinal and transverse edges will be given loading with boundary conditions referring to Figure 7(c) as done by [18]. The selection of boundary conditions is based on their relevance to actual conditions in the form of stiffened panel loading with experimental methods, as carried out by Xu, M. C. and Soares, C. G. [23]. In their study, the longitudinal edge was only given a supported condition so that it was still possible for the edge of the plate to deform rotationally. In addition, the transverse stiffener is given a fix constrained in the lateral direction to provide flexibility to experience deformation in the longitudinal direction.

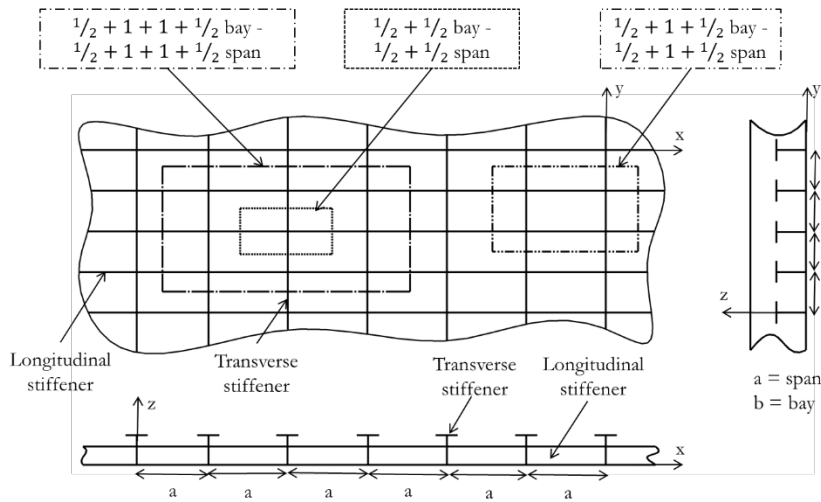


Figure 5: Model range configuration set-up

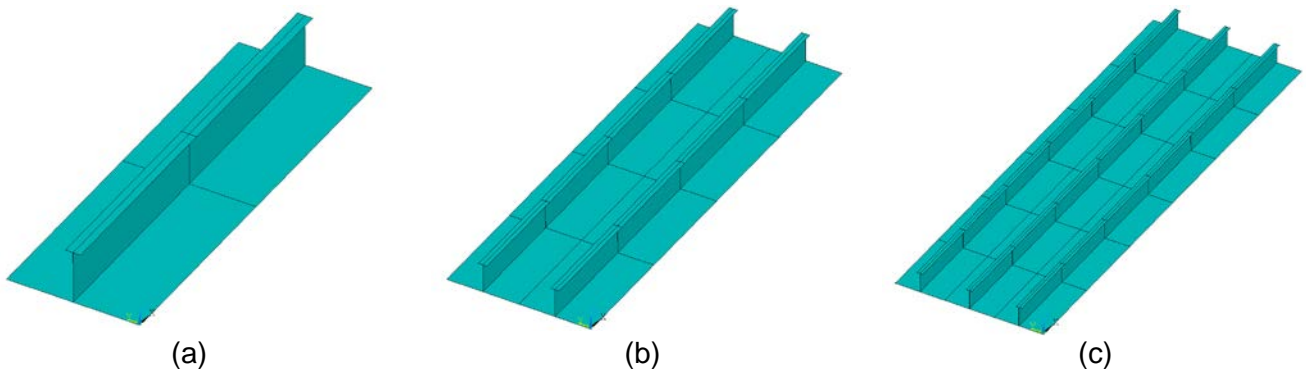


Figure 6: Stiffened panel isometric view, (a) 1/2 + 1/2 bay – 1/2 + 1/2 span, (b) 1/2 + 1 + 1/2 bay – 1/2 + 1 + 1/2 span, (c) 1/2 + 1 + 1 + 1/2 bay – 1/2 + 1 + 1 + 1/2 span

2.4 Boundary condition

Differences in geometry, configuration, and standard guidelines can make the application of boundary conditions diverse. Such a study by Anyfantis [8] considered the effect of non-uniform thrust variation. Alternatively, research conducted by Lutfi, Y. M. et al. [17] analyzed the hull section of the OTEC seawater tank due to the effects of compression and imposed displacement. Therefore, in this study, the influence of various boundary conditions will be applied to the modeling 1/2 + 1/2 bay – 1/2 + 1/2 span and by using ANSYS APDL. The modification was done by applying several boundary conditions illustrated in Figures 7(a) – 7(d).

The boundary condition variations in each test conducted by different researchers have their own approaches and advantages. Figure 7(a) represents the use of boundary conditions by Anyfantis [8] using simply supported conditions and allowing rotations at the connection edges to capture the conditions when the model experiences the worst deformation conditions under compression, as happened in actual events. A different way is taken by Lutfi [17] by setting a uniform condition on each connection edge, as shown in Figure 7(b). This condition makes each node on both transverse and longitudinal edges move continuously when the model is loaded in the x-axis direction. In addition, the study applied the load from two opposite directions so that the constraint fix is added to the nodes in the center of the plate so that the deformation remains in accordance with the actual condition. In contrast, Figure 7(c) illustrates the boundary condition used by Adiputra [18] to record the buckling deformation of the stiffened panel, as the model is only loaded from one direction but uses the same approach on each edge in the form of uniform condition. In Figure 7(d), Xu [19] conducted a different investigation by providing a symmetric boundary condition because it increases the modeling uncertainty and provides the most reliable collapse mode and ultimate strength. Imposed compressive displacement in the x-axis will be applied to all models to capture the buckling capability of each stiffened panel. Models B1 and B3 are given a compressive displacement from one side, with the other side being fixed constraint. Similar to these two models, model B4 is also assigned a displacement from one side, but the compressive displacement is only exerted on the plate. While in model B2, as mentioned earlier, the imposed displacement is induced at the nodes at the end of the plate on both sides since the uniform condition is applied on all sides.

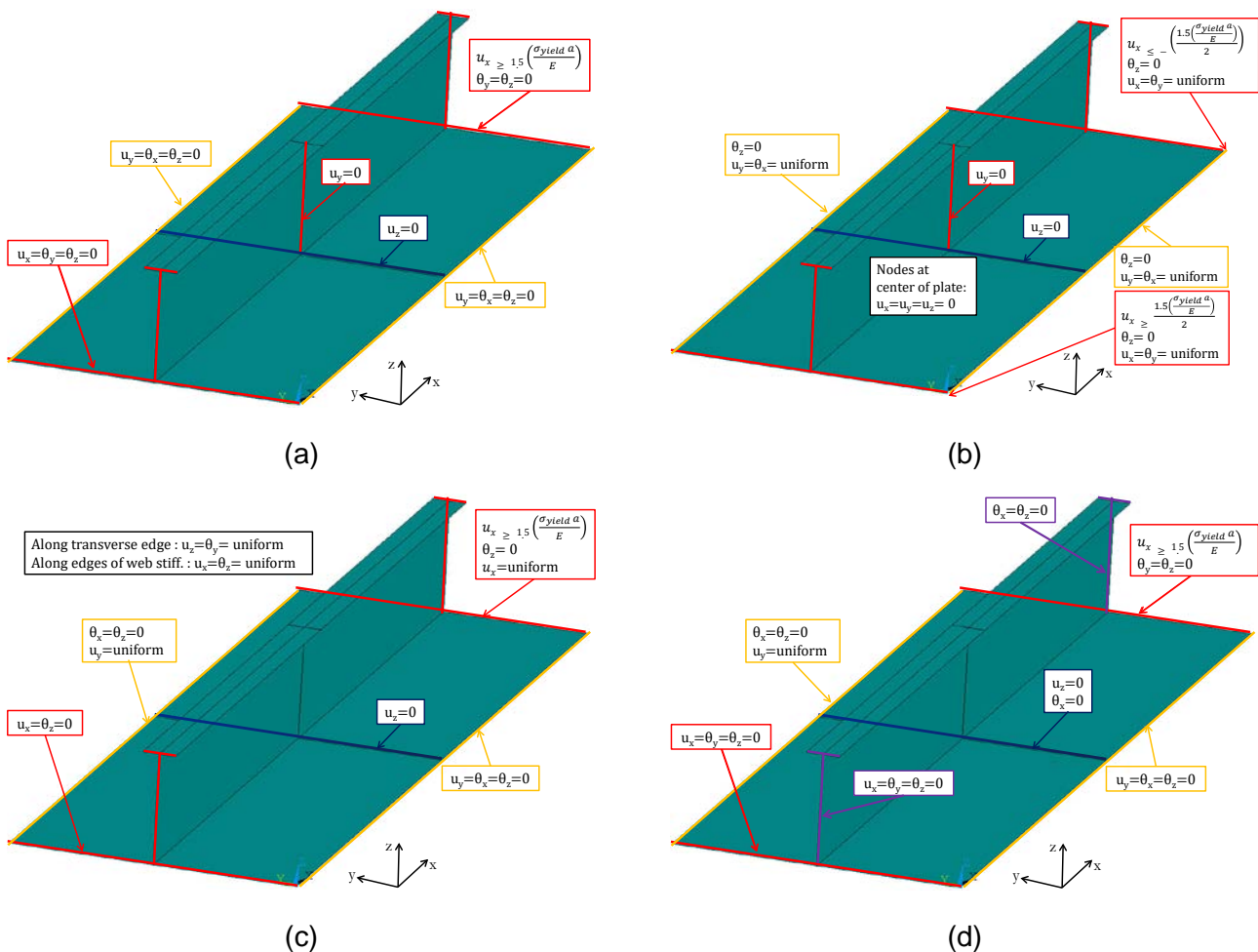


Figure 7: Applied boundary conditions and given loading from reference studies. (a) Anyfantis (B1) [8], (b) Lutfi et al. (B2) [17], (c) Adiputra et al. (B3) [18], (d) Xu et al. (B4) [19]

2.5 Transverse stiffener modelling

To determine the effect of the transverse stiffener, stiffened panel modeling was carried out by modeling it in 3D. A parametric study compared the model with the transverse stiffener with the model without the transverse stiffener or C1 and the dimensional variation of the transverse stiffener. To determine the effect of transverse stiffener modeling, all geometries are assumed to be the same for the plate and longitudinal stiffener. The model with the first transverse stiffener, or C2, as shown in Table 3, will have the exact dimensions of the longitudinal stiffener. Transverse stiffeners in C3 and C4 models will have a more significant moment of inertia than longitudinal stiffeners, based on actual conditions on the ship [6]. For the same reason, the model will also be given the same boundary conditions in model configuration variations by modifying the transverse stiffener. However, there is a difference that does not provide a fixed constraint on the displacement in the z-axis in the transverse stiffener except for the C1 model. This is because transverse stiffeners have been modeled in 3D. The modeling of the transverse stiffener geometry on C2, C3, and C4 is based on a study conducted by Platypodis and Anyfantis [6]. In this case, further research was conducted to determine the most optimal and efficient use in determining the strength of the stiffened panel.

Table 3: Detailed dimensions of transverse stiffener modeling variations

Model	Transverse stiffener dimensions (mm)
C1	N/A
C2	333 X 9 + 100 X 16
C3	360 X 16 + 120 X 16
C4	400 X 17 + 140 X 17

2.6 Initial imperfection geometrics

The comparison of ultimate strength results is one of the analyses that will be carried out, so it is vital to provide the effect of initial imperfection geometrics because it will significantly affect the ultimate value obtained [24-25]. Imperfection buckling mode was given in this study to trigger the type of collapse(s) that will occur in stiffened panels when subjected to uniform thrust loading. The form of collapse(s) mode that was varied this time was a mathematical function and consisted of local and global buckling modes, as formulated in Eqs. 1-3 and illustrated in Figure 8.

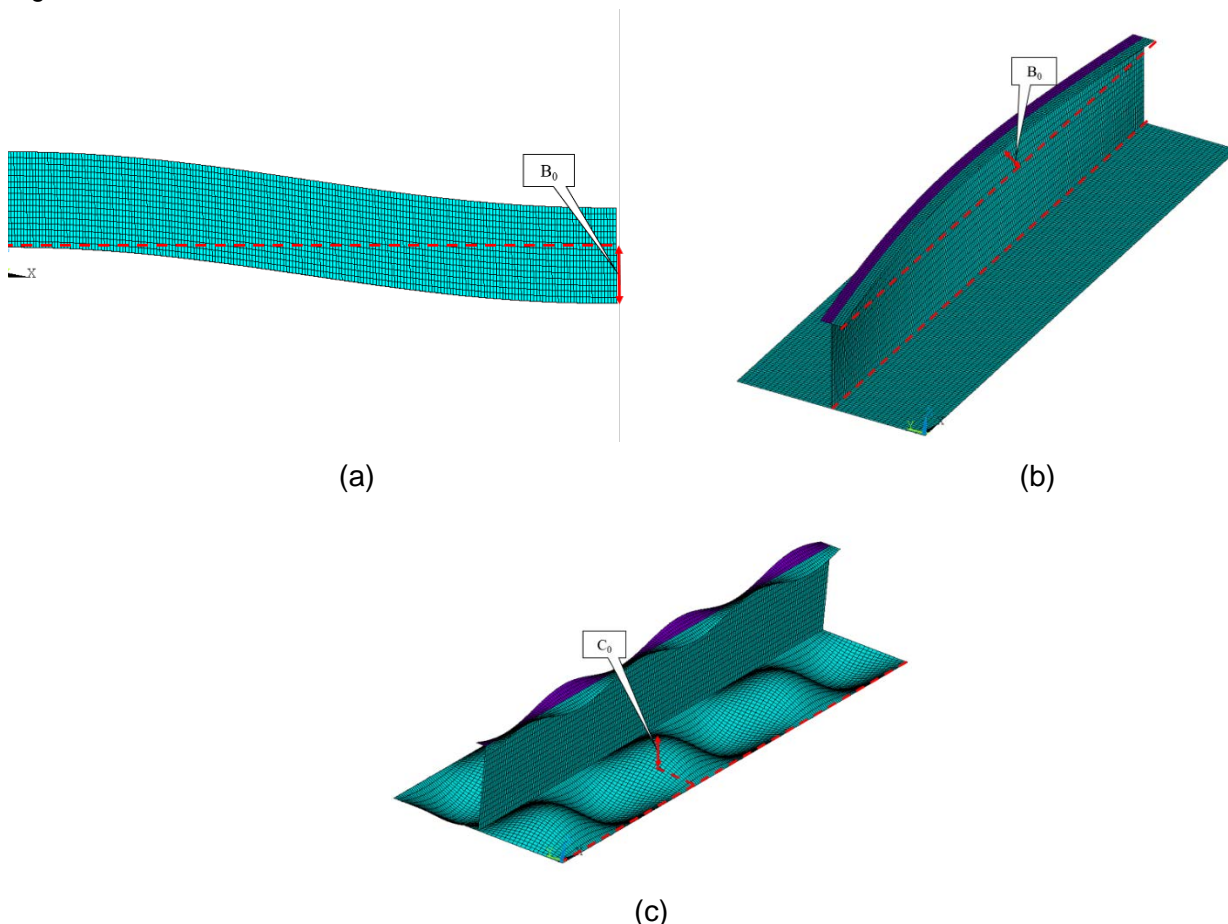


Figure 8: Typical imperfections buckling modes applied on all models, (a) Column imperfection mode, (b) Torsional imperfection mode, (c) Local imperfection mode

– Column imperfection mode

Column imperfection buckling mode is a global buckling mode that explains that all parts on the stiffened panel, both plate and stiffener, experience geometrical imperfection.

$$W_c = B_0 \sin \frac{\pi x_i}{a} \quad (1)$$

– Torsional imperfection mode

Torsional, or can also be called stiffener local buckling, is one type of local imperfection buckling that will be applied to the stiffener in the form of torsional distortion.

$$W_t = B_0 \frac{z_i}{h_s} \sin \frac{\pi x_i}{a} \quad (2)$$

– Local imperfection mode

The local imperfection mode referred to in this section is the local buckling mode that occurs on the plate as an influence of geometric shapes on the x and y axes.

$$W_l = C_0 \sin \frac{m\pi x_i}{a} \sin \frac{\pi y_i}{b} \quad (3)$$

The value of m in Eq. 3 defines the value of the critical half-wave number and is formulated by comparing the value with the span/bay ratio, as in Eq. 4.

$$a/b \leq \sqrt{m^2 + m} \quad (4)$$

The amplitude value in the form of B_0 and C_0 in each type of imperfection mode is a calculation that represents the actual condition of the ship. This value is more deeply described in [8 & 26] studies. The value of B_0 is a function of the bay dimension, while C_0 is a function of plate thickness and the square of the ratio plate slenderness, as written in Eq. 7.

$$B_0 = 0.1 \left(\frac{b}{1000} \right) \quad (5)$$

$$C_0 = 0.1(\beta_p^2 t_p / 10) \quad (6)$$

$$\text{Plate slenderness ratio} = \beta_p = \frac{b}{t_p} \sqrt{\frac{\sigma_{yield}}{E}} \quad (7)$$

The division of the number of element divisions applied to the stiffened panel with a configuration of 1 bay – 1 span is illustrated in Figure 9. The division of the number of elements and the meshing setting will increase with the size of the range configuration model, as illustrated in Figure 5.

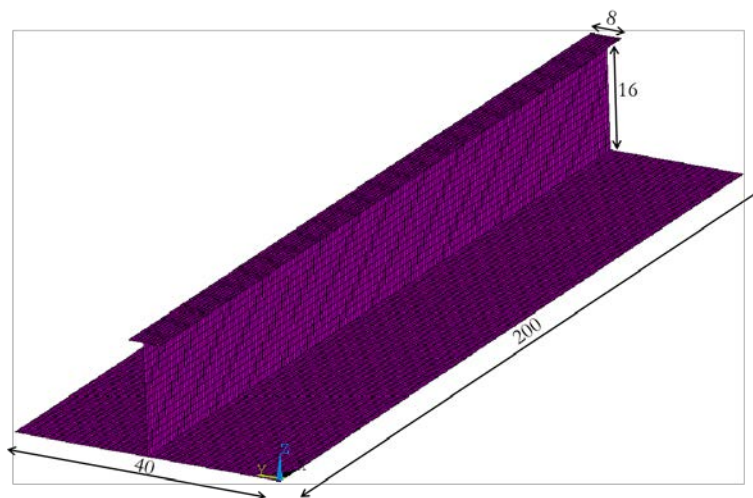


Figure 9: Illustration of the number of element divisions applied on stiffened panels

A large strain shell composed of four nodes was selected for the modeling. As shown in Figure 10 [27], where r, s, and t represent degrees of freedom in the form of translational motion, u, v, and w indicate that this type of shell can move in the direction of rotation. Type "Shell-181", also used by [28-36] in evaluating stiffened panels and various thin-walled and curved-layered structures, explained that the whole type of motion works on a 3-dimensional scope. Therefore, a total of 6 DOF with the type of model material in the form of bilinear isotropic hardening compiles a model to describe plastic deformation when subjected to an external force. Failure mechanism on the stiffened panel was measured by recording the trend of the strain-stress graph with regard to the ultimate limit state for

measuring the strength of each parametric study model. Besides the ultimate strength value, the failure mechanism in each model was studied based on the contour pattern in each phase when the displacement was imposed.

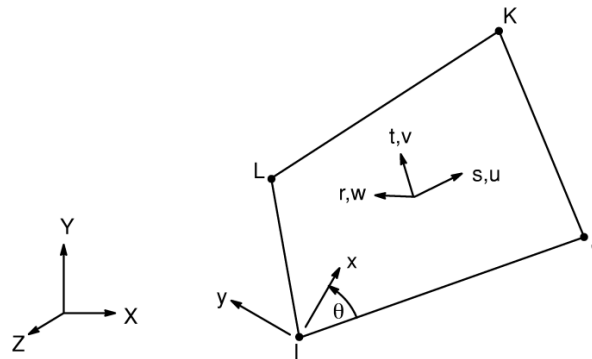


Figure 10: The number of DOF of "Shell 181" - Large strain shell

3 RESULTS AND DISCUSSION

3.1 Model configuration

The stress-relative strain curves of models A1, A2, and A3 under uniform thrust loading were depicted, showcasing the influence of varying the model's range configuration, as presented in Figure 11. The graph also shows specific points referenced in Table 4, which displays the contour of Von Mises. It can be seen that the greatest ultimate value belonged to the most extensive range configuration model, the A3 model, with a value of 288.96 MPa. While on the contrary, the model with the smallest configuration had the smallest ultimate value with a difference of about 37 MPa. This difference is more clearly illustrated in Table 4.

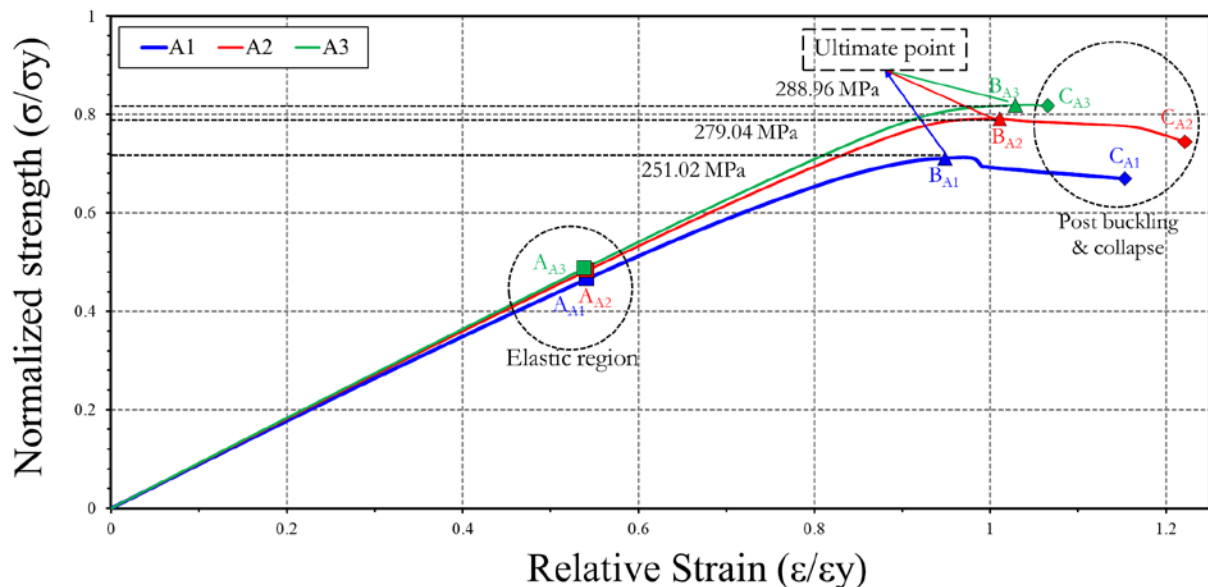
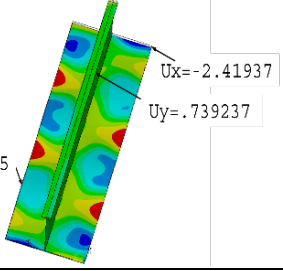
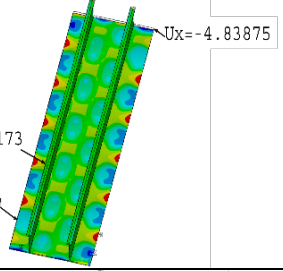
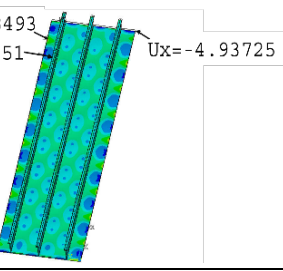
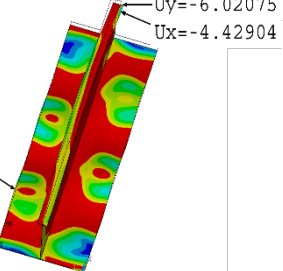
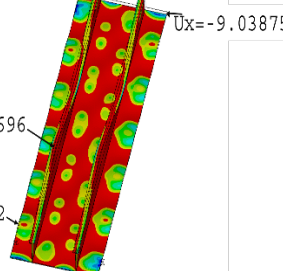
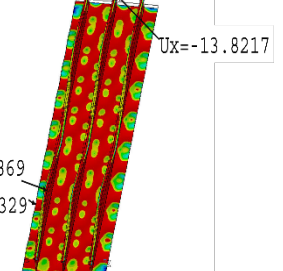
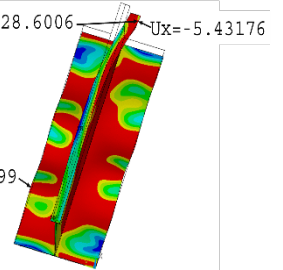
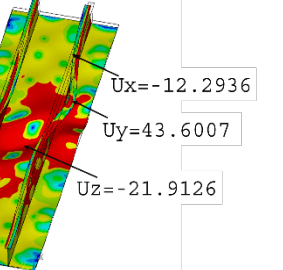
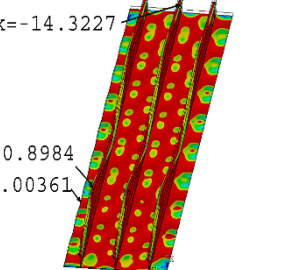
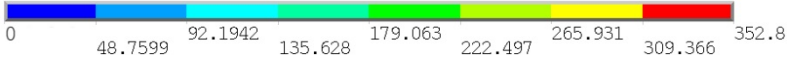


Figure 11: Stress – relative strain curves of related model configuration parameters

The stiffened panel's response could affect the difference in stress-relative strain curves and ultimate strength values. The effect of the initial imperfection geometric in the form of buckling mode also began to influence when the entire stiffened panel was in the elastic region. Local plate buckling became the most dominant which was marked on the Von Mises phase A contour. The imposed displacement in the x-axis direction also made the stiffener experience torsion in the y-axis direction due to the influence of the torsional imperfection mode. Model A1 only experienced a slight deformation of about 6 mm, while models A2 and A3 are about 12 and 15 mm, respectively. Based on Table 4, the deformation of the longitudinal stiffener occurred in the portion that was not supported by the transverse stiffener as shown when the models reached phase B (the ultimate point) and C (post-buckling). As shown in model A1, the stiffener experienced the largest deformation at the end of the stiffener, while models A2 and A3 experienced it in certain areas along the longitudinal stiffener. It is clearly shown in model A2 where the region started from the center of the longitudinal stiffener to near the transverse stiffener experienced the largest deformation. It occurred because of the constraints' effect on the center area of the longitudinal stiffener that represented the transverse stiffener. Although it had the same end-to-end in the form of $1/2 + 1/2$, the presence of 1 span intact on the A2 and A3 models in the middle of the model causes torsional buckling to occur more significantly. In addition, the shape of the critical half wave at the initial geometric imperfection due to the span length also affected the shape of the resulting buckling mode. In phase B, column buckling also afflicted all models and became more visible in phase C, especially in model A1.

However, the failure mechanism and mode mentioned before in the local plate, stiffener torsion, and column buckling indicated that one model had presented results in line with other models. It can be seen in phase B for model A1 where the contour shown was in agreement with the results in the model with a larger scope. The number of local buckling modes shown current condition along the span of 3 also showed consistency with the results shown in the same phase in model A2 and A3, which showed multiple of 6 and 9, respectively. The failure mechanism showed that each model had similarities in producing contour patterns, and the smallest model configuration can produce results that agreed with actual conditions in a simple form.

Table 4. Von Misses of related transverse stiffener modeling parameters

Model \ Phase	A1	A2	A3
A	 <p> $U_x = -2.41937$ $U_y = .739237$ $U_z = -3.06345$ </p>	 <p> $U_x = -4.83875$ $U_y = 1.11173$ $U_z = 2.66497$ </p>	 <p> $U_z = -1.68493$ $U_y = .872451$ $U_x = -4.93725$ </p>
B	 <p> $U_y = -6.02075$ $U_x = -4.42904$ $U_z = 7.0817$ </p>	 <p> $U_x = -9.03875$ $U_y = 12.2696$ $U_z = 6.77702$ </p>	 <p> $U_x = -13.8217$ $U_y = 15.8869$ $U_z = -6.65329$ </p>
C	 <p> $U_y = -28.6006$ $U_x = -5.43176$ $U_z = 10.1399$ </p>	 <p> $U_x = -12.2936$ $U_y = 43.6007$ $U_z = -21.9126$ </p>	 <p> $U_x = -14.3227$ $U_y = 20.8984$ $U_z = -8.00361$ </p>
 <p>0 48.7599 92.1942 135.628 179.063 222.497 265.931 309.366 352.8</p>			

3.2 Boundary condition

A variation in the ultimate strength value was observed among different models with varying boundary conditions, as depicted in the results presented in Figure 12. However, the differences that occurred did not have a distance of values that differed much. The most significant difference between the two models occurred in model B1 with model B4 with a difference in value of only about 15 MPa. Each boundary condition applied to the model represented the corresponding result.

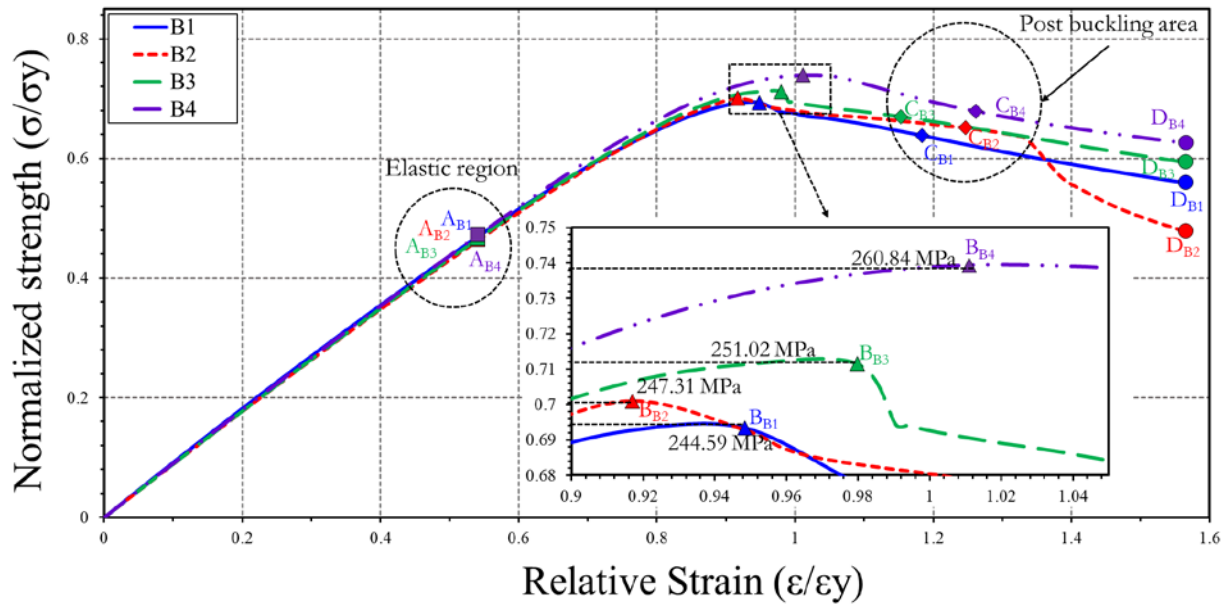
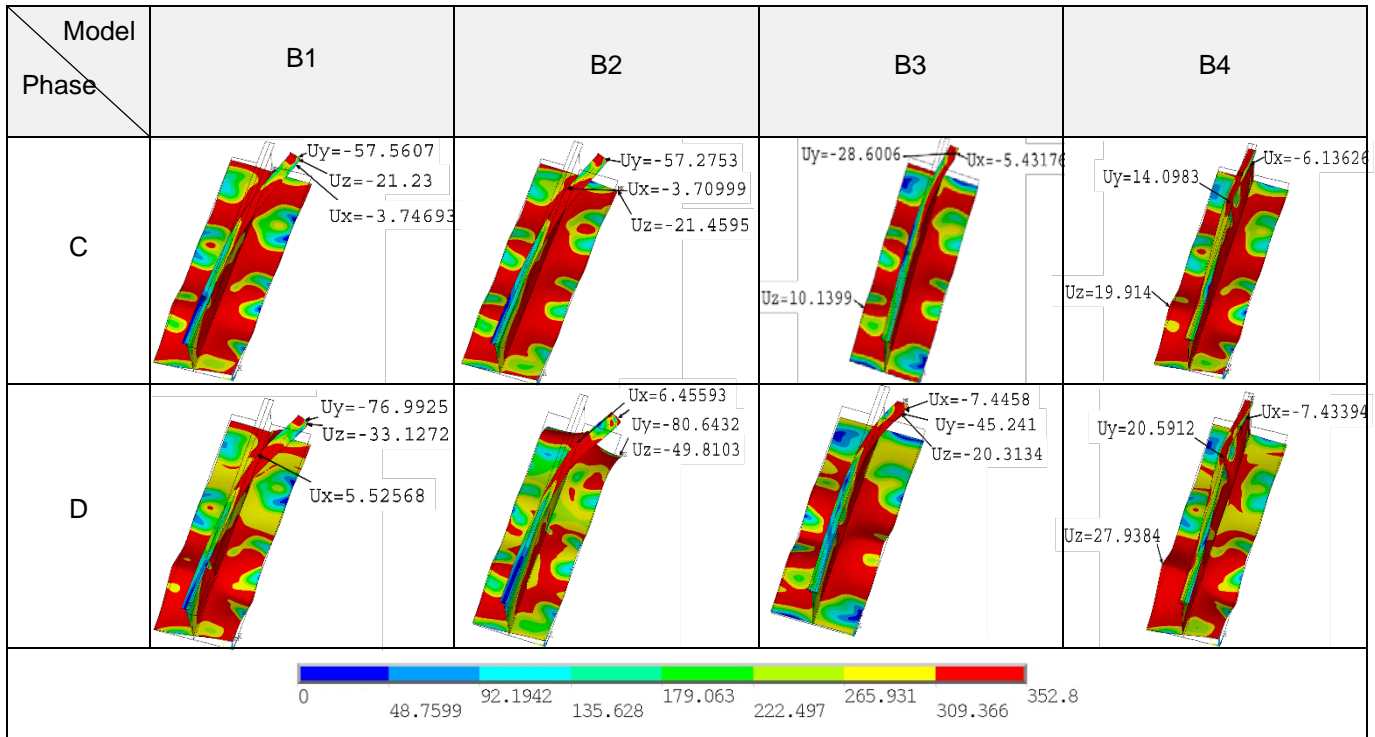


Figure 12: Stress – relative strain curves of related boundary condition parameters

Even so, the difference in boundary conditions would show a different response of the failure mechanism to the stiffened panel shape when loaded, as shown in Table 5. Models B1, B2, and B3 showed significant torsional buckling from phase B (ultimate point) to D (collapse). Nevertheless, in the B4 model, this did not happen because of the fixing constraints on the rotational motion on the x-axis. It caused no deformation of the y-axis that occurred in the stiffener. Not only torsional deflection but also local and column buckling occurred in the stiffened panel due to the influence of local and column imperfection modes. Similar to the previous parameter, local plate buckling had an effect earlier than column and torsional buckling, which was visible when the model reached the ultimate point or phase B. In the C and D phases, the B2 model's plate showed different deformation that experienced significant deformation on the z-axis, caused by displacement conditions on rotation on the x-axis only given uniform conditions. In addition, the post-buckling and collapse phases indicated that allowing individual edges of the B2 model to experience rotational deformation caused the effects of the column imperfection mode to be significant. Thus, based on the results shown in Table 5, the model B2 approach showed a good agreement with the actual conditions because it allowed rotational deformations, which might occur at every edge along the stiffener and the plate. Providing boundary conditions in the form of uniform conditions on each edge allowed for the worst possible deformation, which resulted in the most suitable boundary condition setting to analyze the stiffened panel.

Table 5. Von Misses of related transverse boundary condition parameters

Model \ Phase	B1	B2	B3	B4
A	 $U_y = -1.84972$ $U_x = -1.20969$ $U_z = -3.40096$	 $U_y = -1.22791$ $U_x = -1.20969$ $U_z = 2.68873$	 $U_x = -2.4193$ $U_y = .739237$ $U_z = -3.06345$	 $U_z = -2.73853$ $U_x = -2.41937$ $U_y = .651456$
B	 $U_y = -15.4916$ $U_x = -2.21347$ $U_z = -8.53909$	 $U_y = -8.52974$ $U_x = -2.05109$ $U_z = -6.12179$	 $U_y = -6.02079$ $U_x = -4.42904$ $U_z = 7.0817$	 $U_y = 4.59048$ $U_x = -4.51937$ $U_z = 7.53608$



3.3 Transverse frame modeling

A comparison of transverse stiffener modeling and shape variation was carried out in this study, with a graph between stress and relative strain presented in Figure 13. The difference in ultimate strength values of about 9 MPa occurred between the C1 model and the model that models transverse stiffeners, namely C2, C3, and C4. The value indicated that the graph and the resulting value did not make a significant difference even without modeling. In addition, geometric variations of the transverse stiffener also showed a relatively small difference, where the most prominent difference occurred between C2 and C4 models with a difference of less than 0.5 MPa. Both of these things showed that a transverse stiffener did not have much effect on the stiffened panel when subjected to uniform thrust loads.

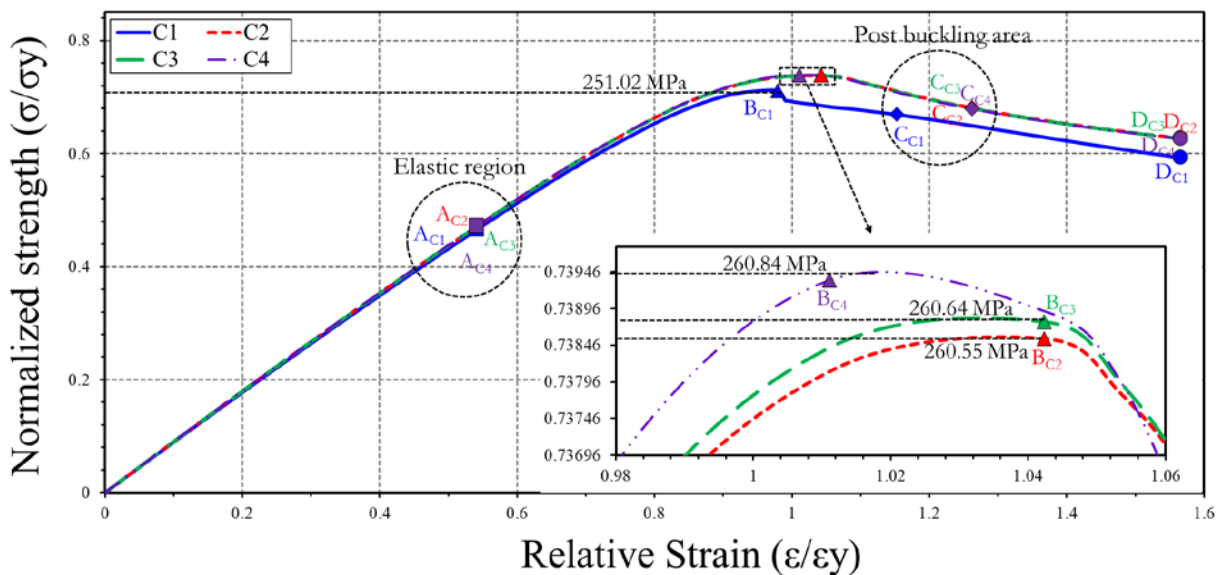
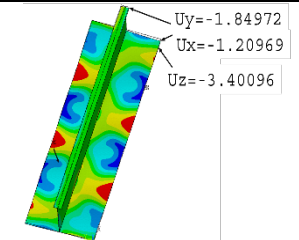
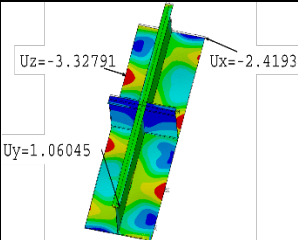
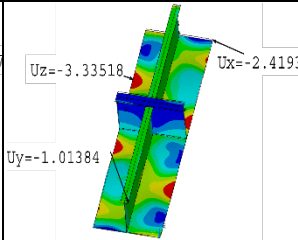
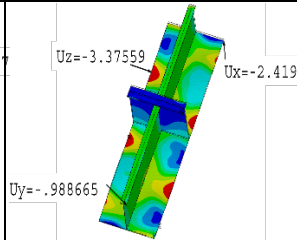
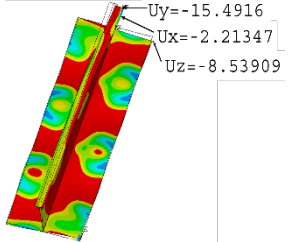
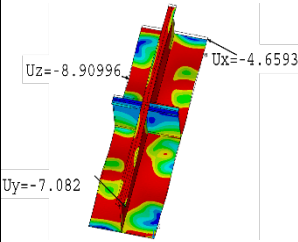
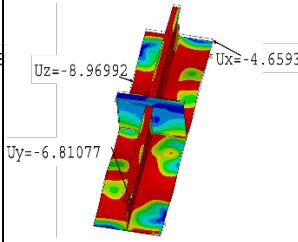
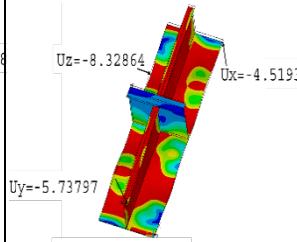
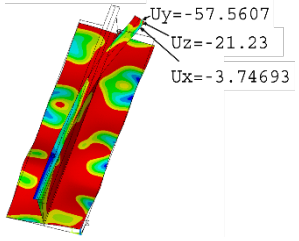
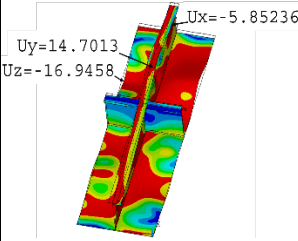
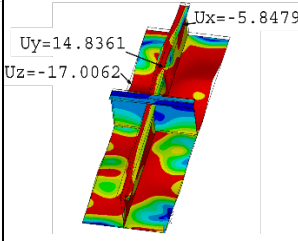
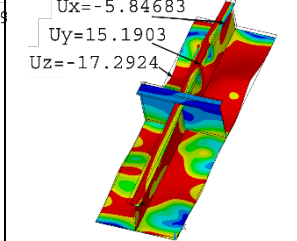
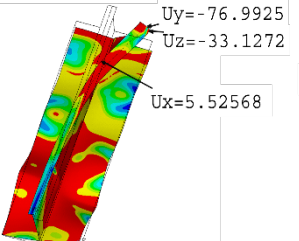
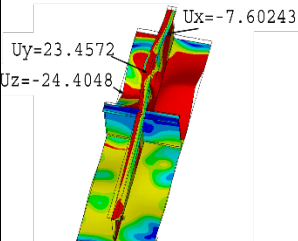
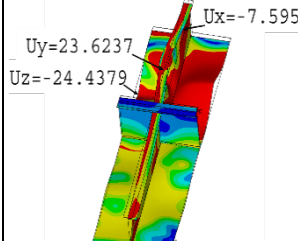
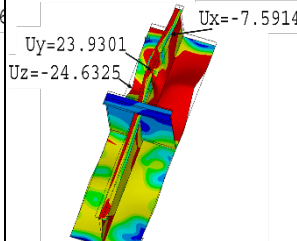
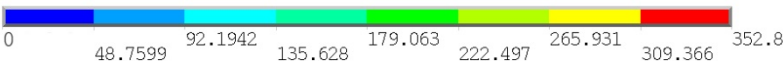


Figure 13: Stress – relative strain curves of related transverse stiffener modeling parameters

As described earlier, there was no big difference in modifying the geometry of the transverse stiffener. Significant differences occurred when comparing the C1 model with other models and this condition obviously showed when all models reached phase B, C, and D which were described as ultimate point, post buckling condition, and collapse condition, respectively. In the C1 model, the longitudinal stiffener underwent considerable deformation with respect to the y-axis; in other models, this deformation did not occur. The most significant deformation in models C2, C3, and C4 was seen on the plate or experiencing local plate buckling. It can be seen in the condition of reaching the ultimate point until collapse from phase C to D that the greater the inertia area of the transverse stiffener made the failure mechanism in the form of deformation of the plate greater even though the difference was relatively slight. It was mainly due to the ability of the plate to continue the imposed displacement restrained by the transverse stiffener so the local buckling dominantly occurred on one side of the stiffened panel separated by the transverse stiffener. The

effect of the local imperfection mode also made the condition worse so that the local plate buckling became more dominant. In contrast, C1 was able to transmit the load so that the buckling on the plate can be evenly distributed. Another distinction was shown in the stiffener where C1 experienced the largest stiffener deformation at the edge while the other three models experienced deformation in the region between one edge and the transverse stiffener. Based on Table 6, modeling the transverse stiffener was not able to distribute the imposed displacement on the plate and stiffener and reduced the effect due to the initial imperfection geometric influence.

Table 6. Von Misses of related transverse stiffener modeling parameters

Model Phase	C1	C2	C3	C4
A	 Uy=-1.84972 Ux=-1.20969 Uz=-3.40096	 Uz=-3.32791 Ux=-2.41937 Uy=1.06045	 Uz=-3.33518 Ux=-2.41937 Uy=-1.01384	 Uz=-3.37559 Ux=-2.41937 Uy=-.988665
B	 Uy=-15.4916 Ux=-2.21347 Uz=-8.53909	 Uz=-8.90996 Ux=-4.65938 Uy=-7.082	 Uz=-8.96992 Ux=-4.65938 Uy=-6.81077	 Uz=-8.32864 Ux=-4.51937 Uy=-5.73797
C	 Uy=-57.5607 Uz=-21.23 Ux=-3.74693	 Uy=14.7013 Uz=-16.9458 Ux=-5.85236	 Uy=14.8361 Uz=-17.0062 Ux=-5.84799	 Uy=15.1903 Uz=-17.2924 Ux=-5.84683
D	 Uy=-76.9925 Uz=-33.1272 Ux=5.52568	 Uy=23.4572 Uz=-24.4048 Ux=-7.60243	 Uy=23.6237 Uz=-24.4379 Ux=-7.5956	 Uy=23.9301 Uz=-24.6325 Ux=-7.59149
				

3.4 Running time

In conducting analysis using FEM, it is essential to determine the efficiency of the time used when running simulations. It becomes vital when done with a large variety of modeling and requires extensive data, including when analyzing stiffened panels. Time efficiency will be a consideration in addition to other parameters affecting the calculation results. Figure 14 shows the time consumed when calculating the overall variation made in this study.

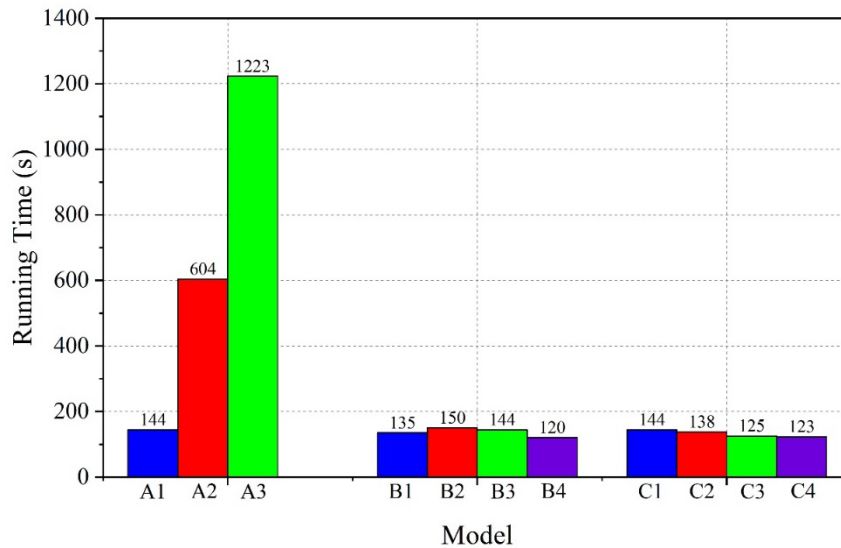


Figure 14. Running time consumed on each model

In model configuration variations, the larger the range configuration model used, the greater the time needed to perform the analysis. The time difference was significant from the A1 to A2 model, with an increase of about six times more significant and 12 times greater than A1 to A3. The time difference was relatively small in modifying boundary conditions and transverse stiffeners. In boundary condition variations, the boundary conditions of Lutfi et al. [17] and Xu et al. [19], respectively. Meanwhile, in the transverse stiffener variation, the graph showed that the larger the geometry of the transverse stiffener consumes, the less time it would consume. The concept of reducing simulation time while maintaining calculation accuracy may be extended to computationally simulate structures made of sophisticated materials such as composites, graphene, and so on [37-42]. Furthermore, the effects of materials under harsh environment [43-50], such as cold region and corrosive-prone water area are potentially to be used as material properties to develop rapid-estimating mathematical forms of structural behaviors based on the potentially sailing routes.

4 CONCLUSIONS

This study has represented a comprehensive parametric investigation to evaluate each parameter in analyzing stiffened panels using the Finite Element Method (FEM). The parametric study was conducted by comparing several variations of model configurations, boundary conditions, and transverse stiffener modeling that were currently developed and used by researchers. In addition, an evaluation of the time efficiency used during numerical calculation running was also conducted to determine the most efficient modeling arrangement. By focusing on numerical methods that provide high accuracy, the study offered a valuable guideline for researchers to determine the most suitable and efficient method. As a result, the investigation provided several conclusions that led to further development in the analysis of stiffened panels through FEM:

- The variation in the ultimate strength value resulted from differences in the range configuration model, boundary conditions, and transverse stiffener modeling was relatively negligible, indicating the overall appropriateness of the variations.
- The most significant difference in the ultimate strength value occurred in the modification of the range configuration model due to the influence of the stiffened panel response when subjected to uniform thrust and the effect of one bay-span structure in the middle of the model section on the stiffened panel with configurations of $1/2 + 1 + 1/2$ and $1/2 + 1 + 1 + 1/2$.
- The configuration model with $1/2 + 1/2$ bay and $1/2 + 1/2$ span, employing boundary conditions with uniform conditions on each side of the stiffened panel and assuming fixed constraint conditions for the transverse stiffeners, is recommended as a valuable guideline for conducting FEM analysis due to its capability in enabling actual deformation of the stiffened panel with minimal time consumption.
- In future studies, it is recommended to analyze the effect of one modeling variation with the other modeling variations on each different parameter to determine the pattern of the ultimate strength value and the contour shape formed on the stiffened panel when subjected to loading.

5 REFERENCES

- [1] O. Mouhat, A. Khamlichi, A. Limam, Assessing buckling strength of stiffened plates as affected by localized initial geometric imperfections, *Int. Rev. Appl. Sci. Eng.* 4 (2013) 97–103.
<https://doi.org/10.1556/irase.4.2013.2.1>.

- [2] C. Wei, G. Wang, M. Cridland, D.L. Olson, S. Liu, Corrosion protection of ships, In Handbook of Environmental Degradation of Materials (William Andrew Publishing, 2018), pp. 533-557. <https://doi.org/10.1016/B978-0-323-52472-8.00026-5>.
- [3] T. Nwigwe, M. Kiyokazu, Statistical Analysis of Bulk Carrier Accident from 2011 to 2020, *TransNav: Int. J. Mar. Nav. Saf. Sea Transp.* 16 (2022). <https://doi.org/10.12716/1001.16.01.18>.
- [4] S.E. Roberts, S.J. Pettit, P.B. Marlow, Casualties and loss of life in bulk carriers from 1980 to 2010, *Mar. Policy* 42 (2013) 223–235. <https://doi.org/10.1016/j.marpol.2013.02.011>.
- [5] Z. Kaddour, Bulk carriers disasters: loading problems and solutions for increased safety at sea. (1998). https://commons.wmu.se/cgi/viewcontent.cgi?article=2063&context=all_dissertations
- [6] E.L. Platypodis, K.N. Anyfantis, On the Modeling of Ship Stiffened Panels Subjected to Uniform Pressure Loads, *Appl. Mech.* 3 (2022) 125–143. <https://doi.org/10.3390/applmech3010010>.
- [7] F.A. Nugroho, B. Siregar, G.L. Putra, R. Dhelika, Study on the alteration of geometrical dimensions of tee stiffeners concerning the ultimate strength characteristics under a vertical bending load, *Int. J. Tech* 9 (2018) 1027–1038. <https://doi.org/10.14716/ijtech.v9i5.1103>.
- [8] K.N. Anyfantis, Ultimate strength of stiffened panels subjected to non-uniform thrust, *Int. J. Naval Archit. Ocean Eng.* 12 (2020) 325–342. <https://doi.org/10.1016/j.ijnaoe.2020.03.003>.
- [9] Y.T. Lin, Ship longitudinal strength modelling (Doctoral dissertation, ProQuest Dissertations & Theses). (1985). <https://theses.gla.ac.uk/77347/>
- [10] J.K. Paik, A.K. Thayamballi, An empirical formulation for predicting the ultimate compressive strength of stiffened panels, In The Seventh International Offshore and Polar Engineering Conference, OnePetro. (1997).
- [11] S. Zhang, I. Khan, Buckling and ultimate capability of plates and stiffened panels in axial compression, *Mar. Struct.* 22 (2009) 791–808. <https://doi.org/10.1016/j.marstruc.2009.09.001>.
- [12] D.K. Kim, H.L. Lim, M.S. Kim, O.J. Hwang, K.S. Park, An empirical formulation for predicting the ultimate strength of stiffened panels subjected to longitudinal compression, *Ocean Eng.* 140 (2017) 270–280. <https://doi.org/10.1016/j.oceaneng.2017.05.031>.
- [13] M.C. Xu, Z.J. Song, B.W. Zhang, J. Pan, Empirical formula for predicting ultimate strength of stiffened panel of ship structure under combined longitudinal compression and lateral loads, *Ocean Eng.* 162 (2018) 161–175. <https://doi.org/10.1016/j.oceaneng.2018.05.015>.
- [14] International Association of Classification Societies (IACS), Common Structural Rules for Bulk Carriers and Oil Tankers. (2022).
- [15] Y.Z. Yu, G.Q. Feng, C.F. Li, H.L. Ren, Experimental and numerical investigation on the ultimate strength of stiffened plates with scanned initial geometrical imperfection, *China Ocean Engineering*, 33 (2019) 446–458. <https://doi.org/10.1007/s13344-019-0042-4>.
- [16] C.L. Yu, Y.T. Chen, S. Yang, Y. Liu, G.C. Lu, Ultimate strength characteristic and assessment of cracked stiffened panel under uniaxial compression, *Ocean Engineering*, 152 (2018) 6–16. <https://doi.org/10.1016/j.oceaneng.2018.01.015>.
- [17] Y.M. Lutfi, R. Adiputra, A.R. Prabowo, T. Utsunomiya, E. Erwandi, N. Muhayat, Assessment of the stiffened panel performance in the OTEC seawater tank design: Parametric study and sensitivity analysis, *Theoretical and Applied Mechanics Letters*, p.100452 (2023). <https://doi.org/10.1016/j.taml.2023.100452>.
- [18] R. Adiputra, T. Yoshikawa, E. Erwandi, Reliability-based assessment of ship hull girder ultimate strength, *Curved and Layered Structures*, 10(1) (2023) 20220189. <https://doi.org/10.1515/cls-2022-0189>.
- [19] M.C. Xu, D. Yanagihara, M. Fujikubo, C.G. Soares, Influence of boundary conditions on the collapse behaviour of stiffened panels under combined loads, *Marine structures*, 34 (2013) 205–225. <https://doi.org/10.1016/j.marstruc.2013.09.002>.
- [20] T. Yao, On loading and boundary conditions for buckling/plastic collapse analysis of continuous stiffened plate by FEM, In 12th Asian Technical Exchange and Advisory Meeting on Marine Structures, TEAM'98 (1998) 305–314. https://doi.org/10.2534/jjasnaoe1968.2000.188_479.
- [21] H. Ohtsubo, Y. Sumi, Proceedings of the 14th International Ship and Offshore Structures Congress, Elsevier Science, Oxford, United Kingdom (2000).
- [22] G.J. Shi, D.W. Gao, Analysis of hull girder ultimate strength for cruise ship with multi-layer superstructures, *Ships and Offshore Structures*, 14(7) (2019) 698–708. <https://doi.org/10.1080/17445302.2018.1552548>.
- [23] M.C. Xu, C.G. Soares, Experimental evaluation of the ultimate strength of stiffened panels under longitudinal compression, *Ocean Engineering*, 220 (2021) 108496. <https://doi.org/10.1016/j.oceaneng.2020.108496>.
- [24] A.P.L. Mateus, Buckling and Ultimate Strength of Stiffened Panel, Técnico Lisboa Thesis Naval Architecture and Ocean Engineering. (2021).
- [25] X. Shi, J. Zhang, A.P. Teixeira, C.G. Soares, Ultimate strength of a stiffened plate with initial imperfections under complex loading, In *Maritime Technology and Engineering* (2014) 503–512.

- [26] M. Fujikubo, T. Yao, M.R. Khedmati, M. Harada, D. Yanagihara, Estimation of ultimate strength of continuous stiffened panel under combined transverse thrust and lateral pressure Part 1: Continuous plate, *Marine Structures*, 18(5-6) (2005) 383–410. <https://doi.org/10.1016/j.marstruc.2005.08.004>.
- [27] P. Kohnke, ANSYS theory reference-Release 5.6, ANSYS. Inc. p.1286 (1999).
- [28] A.R. Prabowo, D.M. Bae, J.H. Cho, J.M. Sohn, Analysis of structural crashworthiness and estimating safety limit accounting for ship collisions on strait territory, *Latin American Journal of Solids and Structures*, 14 (2017) 1594–1613. <https://doi.org/10.1590/1679-78253942>.
- [29] A.R. Prabowo, T. Muttaqie, J.M. Sohn, D.M. Bae, Nonlinear analysis of inter-island roro under impact: Effects of selected collision's parameters on the crashworthy double-side structures, *Journal of the Brazilian Society of Mechanical Sciences and Engineering*, 40 (2018) 248. <https://doi.org/10.1007/s40430-018-1169-6>.
- [30] F. Morshedsolouk, M.R. Khedmati, Parametric study on average stress-average strain curve of composite stiffened plates using progressive failure method, *Latin American Journal of Solids and Structures*, 11 (2014) 2203–2226. <https://doi.org/10.1590/S1679-78252014001200005>.
- [31] A.R. Prabowo, T. Muttaqie, J.M. Sohn, B.I.R. Harsritanto, Investigation on structural component behaviours of double bottom arrangement under grounding accidents, *Theoretical and Applied Mechanics Letters*, 9 (2019) 50–59. <https://doi.org/10.1016/j.taml.2019.01.010>.
- [32] A.R. Prabowo, D.M. Bae, J.M. Sohn, Comparing structural casualties of the Ro-Ro vessel using straight and oblique collision incidents on the car deck, *Journal of Marine Science and Engineering*, 7 (2019) 183. <https://doi.org/10.3390/jmse7060183>.
- [33] Y. Liu, X. Ji, D. Wang, J. He, Modeling thin structures incorporated with surface effects by using layered shell elements, *European Journal of Mechanics - A/Solids*, 74 (2019) 139–144. <https://doi.org/10.1016/j.euromechsol.2018.11.007>.
- [34] D. Jindra, Z. Kala, J. Kala, S. Seidl, Experimental and Numerical simulation of a Three Point Bending Test of a Stainless Steel Beam, *Transportation Research Procedia*, 55, pp. 1114-1121 (2021). <https://doi.org/10.1016/j.tpro.2021.07.183>.
- [35] M.E. Benincá, R.J. Schmitz, and I.B. Morsch, Numerical simulation of steel-concrete composite beams: updated strategies of finite element modeling, *IBRACON Structures and Materials Journal*, 13, e13510 (2020). <https://doi.org/10.1590/S1983-41952020000500010>.
- [36] A.R. Prabowo, J.M. Sohn, Nonlinear dynamic behaviors of outer shell and upper deck structures subjected to impact loading in maritime environment, *Curved and Layered Structures*, 6, pp. 146–160 (2019). <https://doi.org/10.1515/cls-2019-0012>.
- [37] C.P. Wu, Y.C. Hung, Three-dimensional free vibration analysis of functionally graded graphene platelets-reinforced composite toroidal shells, *Engineering Structures*, 269, 114795 (2022). <https://doi.org/10.1016/j.engstruct.2022.114795>.
- [38] D.F. Smaradhana, A.R. Prabowo, A.N.F. Ganda, Exploring the potential of graphene materials in marine and shipping industries – A technical review for prospective application on ship operation and material-structure aspects, *Journal of Ocean Engineering and Science*, 6, pp. 299–316 (2021). <https://doi.org/10.1016/j.joes.2021.02.004>.
- [39] S. Sakuri, E. Surojo, D. Ariawan, A.R. Prabowo, Experimental investigation on mechanical characteristics of composite reinforced cantala fiber (CF) subjected to microcrystalline cellulose and fumigation treatments, *Composites Communications*, 21, 100419 (2020). <https://doi.org/10.1016/j.coco.2020.100419>.
- [40] R. Wei, K. Shen, G. Pan, A numerical study on the effect of delamination on composite cylindrical shells subjected to hydrostatic pressure, *Ocean Engineering*, 262, 112294 (2022). <https://doi.org/10.1016/j.oceaneng.2022.112294>.
- [41] D. Ariawan, T.S. Rivai, E. Surojo, S. Hidayatulloh, H.I. Akbar, A.R. Prabowo, Effect of alkali treatment of Salacca Zalacca fiber (SZF) on mechanical properties of HDPE composite reinforced with SZF, *Alexandria Engineering Journal*, 59, pp. 3981-3989 (2020). <https://doi.org/10.1016/j.aej.2020.07.005>.
- [42] E.W.A. Fanandi, E. Surojo, A.R. Prabowo, H.I. Akbar, Recent progress in hybrid aluminum composite: Manufacturing and application, *Metals*, 11, 1919 (2021). <https://doi.org/10.3390/met11121919>.
- [43] Y. Xiu, Q. Wang, Z. Li, G. Li, P. Lu, Estimating spatial distributions of design air temperatures for ships and offshore structures in the Arctic Ocean, *Polar Science*, 34, 100875 (2022). <https://doi.org/10.1016/j.polar.2022.100875>.
- [44] K. Riska, R. Bridges, Limit state design and methodologies in ice class rules for ships and standards for Arctic offshore structures, *Marine Structures*, 63, pp. 462-479 (2019). <https://doi.org/10.1016/j.marstruc.2017.09.005>.
- [45] A.R. Prabowo, J.H. Byeon, H.J. Cho, J.M. Sohn, D.M. Bae, J.H. Cho, Impact phenomena assessment: Part I- Structural performance of a tanker subjected to ship grounding at the Arctic, *MATEC Web of Conferences*, 159, 02061 (2018). <https://doi.org/10.1051/matecconf/201815902061>.

- [46] C. Bo, D.M. Bae, J.M. Sohn, A.R. Prabowo, T.H. Chen, H. Li, Numerical analysis for damage characteristics caused by ice collision on side structure, Proceedings of the International Conference on Offshore Mechanics and Arctic Engineering – OMAE, 8, V008T07A019 (2016). <https://doi.org/10.1115/OMAE2016-54727>.
- [47] A.A. Pratama, A.R. Prabowo, T. Muttaqie, N. Muhayat, R. Ridwan, B. Cao, F.B. Laksono, Hollow tube structures subjected to compressive loading: implementation of the pitting corrosion effect in nonlinear FE analysis, Journal of the Brazilian Society of Mechanical Sciences and Engineering, 45, 143 (2023). <https://doi.org/10.1007/s40430-023-04067-3>.
- [48] I. Faqih, R. Adiputra, A.R. Prabowo, N. Muhayat, S. Ehlers, M. Braun, Hull girder ultimate strength of bulk carrier (HGUS-BC) evaluation: Structural performances subjected to true inclination conditions of stiffened panel members, Results in Engineering, 18, 101076 (2023). <https://doi.org/10.1016/j.rineng.2023.101076>.
- [49] D.K. Kim, H.L. Lim, N.K. Cho, An advanced technique to predict time-dependent corrosion damage of onshore, offshore, nearshore and ship structures: Part II = Application to the ship's ballast tank, International Journal of Naval Architecture and Ocean Engineering, 12, pp. 645-656 (2020). <https://doi.org/10.1016/j.ijnaoe.2020.07.002>.
- [50] C. Guedes Soares, Y. Garbatov, A. Zayed, G. Wang, Influence of environmental factors on corrosion of ship structures in marine atmosphere, Corrosion Science, 51, pp. 2014-2026 (2009). <https://doi.org/10.1016/j.corsci.2009.05.028>.

Paper submitted: 30.05.2023.

Paper accepted: 04.08.2023.

This is an open access article distributed under the CC BY 4.0 terms and conditions